A Periodic Array of Parallel Edge Cracks in a Functionally Graded Plate Subjected to Finite Cooling Rates

Yuezhong Feng[1,*], Zhihe Jin[2]

[1] School of Mechanical Engineering, Purdue University, 47907, USA
[2] Department of Mechanical Engineering, University of Maine, 04469, USA
* Corresponding author: feng81@purdue.edu

Abstract This work investigates the effects of cooling rate on the thermal fracture behavior of a functionally graded plate (FGM plate) with a periodic array of parallel edge cracks of alternating lengths. The thermal properties of the FGM are assumed to be continuous and piecewise differentiable functions of the coordinate in the plate thickness direction. A linear ramp function describes the rate of boundary temperature variation at the surfaces of the FGM plate. The integral equation method is used to analyze the thermal stress intensity factors (TSIFs) at the crack tips. The asymptotic solutions of TSIF are obtained using a closed form, short time solution of temperature field in the FGM plate. The effects of cooling rate and crack length ratio on the TSIF are examined using an Al_2O_3/Si_3N_4 FGM. Numerical results show that for given material gradation profile and crack morphology parameters, a lower cooling rate leads to a lower peak TSIF. For a given cooling rate, an appropriate material gradation profile reduces peak TSIFs. Finally, the variations of the TISF for the long and short cracks with the cooling rate and crack length ratio exhibit a complex pattern due to the interactions between the long and short cracks.

Keywords functionally graded material, heat conduction, cooling rate, thermal stress intensity factor, periodic cracks

1. Introduction

Functionally graded ceramics suffer multiple surface cracking when subjected to thermal shocks [1, 2]. These surface cracks greatly influence the thermal fracture behavior of the materials. FGMs with multiple surface cracks under thermal loading were considered by Rangaraj and Kokini [3], Han and Wang [4], and Jin and Feng [5]. Jin and Feng [6] further investigated thermal shock residual strength of an FGM with multiple surface cracks. The existing analytical and computational studies on multiple surface cracking in FGMs have assumed that the cracks have equal length. However, FGMs when subjected to thermal shocks may develop multiple cracks of unequal lengths as in the case of monolithic ceramics. An improved model is a periodic array of parallel cracks with alternating lengths. For monolithic ceramics, Nemat-Nasser et al. [7] considered a periodic array of parallel cracks with alternating lengths in a half plane and studied the stability problem of crack growth. Using a boundary element method and an energy release fracture criterion, Bahr et al. [8] studied the same crack geometry in a plate of finite thickness. Jin and Feng [9] considered an array of parallel edge cracks with alternating lengths in an elastic strip subjected to a thermal shock and presented detailed results on the effects of crack length ratio and crack spacing on the thermal stress intensity factors (TSIFs). For functionally graded ceramics, Feng and Jin [10, 11] investigated the effects of crack length ratio on the TSIFs at the tips of long and short cracks and thermal shock residual strength using a singular integral equation technique.

All of the analytical studies above assume that the FGM specimens are subjected to a sudden cooling condition at their surfaces, i.e., the boundary temperature immediately attains the ambient temperature. In practical applications, however, the cooling rates on the material surfaces are finite.

The objective of this work is to investigate the effects of cooling rate on the TSIFs for an array of parallel edge cracks with alternating lengths in a functionally graded ceramic plate. A linear ramp function is used to describe the rate of boundary temperature variations at the surfaces of the FGM plate. The remainder of the paper is organized as follows. Section 2 reviews a closed-form, asymptotic solution of temperature field for short times and the thermal stresses in the periodically cracked FGM plate. Section 3 describes an integral equation method to obtain the TSIFs at the tips of long and short cracks. Section 4 presents numerical results of TSIFs for an Al_2O_3/Si_3N_4 FGM. Section 5 provides concluding remarks.

2. Temperature and Thermal Stress Fields

This section reviews the temperature and thermal stress solutions for a long FGM plate with an array of parallel edge cracks with alternating lengths as shown in Fig. 1, where a_1 is the length of the long cracks, a_2 is the length of the short cracks, h is the crack spacing, and b is the plate thickness. The thermal properties of the FGM plate are arbitrarily graded in the thickness direction (x-direction). Initially the temperature of the plate is a constant T_0 which can be assumed to be zero without loss of generality. The temperature then gradually changes to $-T_a$ and $-T_b$ at the surfaces $x = 0$ and $x = b$ of the plate, respectively. We use a linear ramp function to describe the variations of the boundary temperatures. The initial and boundary conditions for the heat conduction problem are thus

$$T(x,0) = 0, \qquad 0 \le x \le b, \tag{1}$$

$$T(0,t) = \begin{cases} -T_a\left(t/t_a\right), & 0 \le t \le t_a \\ -T_a, & t > t_a \end{cases}, \tag{2a}$$

$$T(b,t) = \begin{cases} -T_b\left(t/t_b\right), & 0 \le t \le t_b \\ -T_b, & t > t_b \end{cases}, \tag{2b}$$

where $T = T(x, t)$ is the temperature, t is time, and t_a and t_b are two temporal parameters describing the rates of temperature variation (cooling/heating rates) at the plate surfaces. The one-dimensional heat conduction in the plate is governed by the following basic equation

$$\frac{\partial}{\partial x}\left[k(x)\frac{\partial T}{\partial x}\right] = \rho(x)c(x)\frac{\partial T}{\partial t}, \tag{3}$$

where $k(x)$ is the thermal conductivity, $\rho(x)$ the mass density, and $c(x)$ the specific heat.

Jin [12] obtained a closed form solution of the temperature field for short times in the FGM plate with continuous and piecewise differentiable properties as follows

$$\frac{T(x,\tau)}{T_a} = T^{(1)}(x,\tau) + \left(\frac{T_b}{T_a}\right) T^{(2)}(x,\tau), \tag{4}$$

where $T^{(1)}(x,\tau)$ and $T^{(2)}(x,\tau)$ are given by

$$\begin{aligned} T^{(1)}(x,\tau) = &-\frac{1}{\tau_a}\left[\frac{\rho_0 c_0 k_0}{\rho(x)c(x)k(x)}\right]^{1/4} \\ &\times\left\{\left[\tau + \frac{1}{2}\Omega_1^2(x)\right] erfc\left(\frac{\Omega_1(x)}{2\sqrt{\tau}}\right) - \frac{\Omega_1(x)}{\sqrt{\pi}}\sqrt{\tau}\exp\left[-\frac{\Omega_1^2(x)}{4\tau}\right]\right\}, \quad \tau \le \tau_a, \end{aligned} \tag{5a}$$

$$T^{(1)}(x,\tau)=-\frac{1}{\tau_a}\left[\frac{\rho_0 c_0 k_0}{\rho(x)c(x)k(x)}\right]^{1/4}\left\{\left[\tau+\frac{1}{2}\Omega_1^2(x)\right]erfc\left(\frac{\Omega_1(x)}{2\sqrt{\tau}}\right)-\frac{\Omega_1(x)}{\sqrt{\pi}}\sqrt{\tau}\exp\left[-\frac{\Omega_1^2(x)}{4\tau}\right]\right.$$
$$\left.-\left[\tau-\tau_a+\frac{1}{2}\Omega_1^2(x)\right]erfc\left(\frac{\Omega_1(x)}{2\sqrt{\tau-\tau_a}}\right)+\frac{\Omega_1(x)}{\sqrt{\pi}}\sqrt{\tau-\tau_a}\exp\left[-\frac{\Omega_1^2(x)}{4(\tau-\tau_a)}\right]\right\},\quad \tau>\tau_a, \tag{5b}$$

and

$$T^{(2)}(x,\tau)=-\frac{1}{\tau_b}\left[\frac{\rho(b)c(b)k(b)}{\rho(x)c(x)k(x)}\right]^{1/4}$$
$$\times\left\{\left[\tau+\frac{1}{2}\Omega_2^2(x)\right]erfc\left(\frac{\Omega_2(x)}{2\sqrt{\tau}}\right)-\frac{\Omega_2(x)}{\sqrt{\pi}}\sqrt{\tau}\exp\left[-\frac{\Omega_2^2(x)}{4\tau}\right]\right\},\quad \tau\le\tau_b, \tag{6a}$$

$$T^{(2)}(x,\tau)=-\frac{1}{\tau_b}\left[\frac{\rho(b)c(b)k(b)}{\rho(x)c(x)k(x)}\right]^{1/4}\left\{\left[\tau+\frac{1}{2}\Omega_2(x)\right]erfc\left(\frac{\Omega_2(x)}{2\sqrt{\tau}}\right)-\frac{\Omega_2(x)}{\sqrt{\pi}}\sqrt{\tau}\exp\left[-\frac{\Omega_2^2(x)}{4\tau}\right]\right.$$
$$\left.-\left[\tau-\tau_b+\frac{1}{2}\Omega_2^2(x)\right]erfc\left(\frac{\Omega_2(x)}{2\sqrt{\tau-\tau_b}}\right)+\frac{\Omega_2(x)}{\sqrt{\pi}}\sqrt{\tau-\tau_b}\exp\left[-\frac{\Omega_2^2(x)}{4(\tau-\tau_b)}\right]\right\},\quad \tau>\tau_b, \tag{6b}$$

respectively, and τ, τ_a and τ_b are the nondimensional times defined by

$$\tau=t\kappa_0/b^2,\qquad \tau_a=t_a\kappa_0/b^2,\qquad \tau_b=t_b\kappa_0/b^2, \tag{7}$$

in which $\kappa_0=\kappa(0)$ and $\kappa(x)=k/(\rho c)$ is the thermal diffusivity. In Eqs. (5) and (6), *erfc*( ) is the complementary error function and $\Omega_1(x)$ and $\Omega_2(x)$ are defined by

$$\Omega_1(x)=\frac{1}{b}\int_0^x\sqrt{\frac{\kappa_0}{\kappa(x')}}\,dx',\qquad \Omega_2(x)=\frac{1}{b}\int_x^b\sqrt{\frac{\kappa_0}{\kappa(x')}}\,dx'. \tag{8}$$

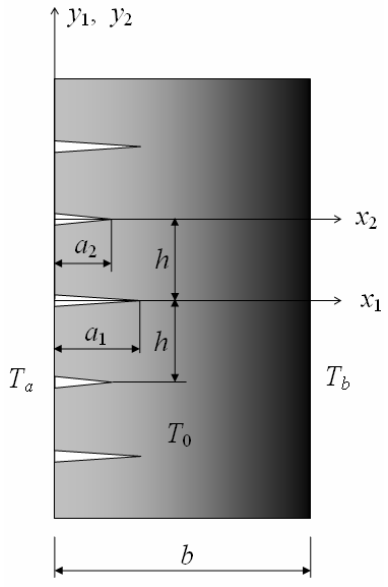

Figure 1. An FGM plate containing an array of periodic edge cracks with alternating lengths subjected to a thermal shock

The above temperature filed induces thermal stresses in both longitudinal (perpendicular to the crack direction) and transverse (perpendicular to the *x*-*y* plane) directions in the FGM plate. The

growth of the periodic edge cracks, however, is caused by the longitudinal stress which has the following form when the cracks have not been considered

$$\sigma_{yy}^{T}(x,\tau)=-\frac{E\alpha\theta(x,\tau)}{1-\nu}+\frac{E}{1-\nu}\left[\left(4-6\frac{x}{b}\right)\frac{1}{b}\int_0^b\alpha\theta(x,\tau)dx-\left(6-12\frac{x}{b}\right)\frac{1}{b^2}\int_0^b\alpha x\theta(x,\tau)dx\right], \quad (9)$$

where $\theta(x,\tau) = T(x,\tau)-T_0$, E is Young's modulus, ν is Poisson's ratio, and $\alpha = \alpha(x)$ is the coefficient of thermal expansion. Here we assume that the FGM plate is thermally nonhomogeneous but elastically homogeneous, i.e., the Young's modulus and Poisson's ratio are constant. While this assumption imposes limitations on the application of the present model, there exist some FGM systems for which the Young's modulus remains approximately constant. Examples include TiC/SiC, $MoSi_2/Al_2O_3$, Al_2O_3/Si_3N_4, and ZrO_2/Nickel FGM systems.

3. Thermal Stress Intensity Factors

This section uses the asymptotic temperature solution (4) – (6) to calculate the thermal stress intensity factor (TSIFs) at the tips of long and short crack in an elastically homogeneous but thermally graded FGM plate (see Fig. 1). The integral equation method is employed and the singular integral equations of the crack problem are given as follows

$$\int_{-1}^{1}\left[\frac{1}{s_1-r_1}+\frac{a_1}{2}k_{11}(r_1,s_1)\right]f_1(s_1)ds_1+\int_{-1}^{1}\frac{a_2}{2}k_{12}(r_2,s_2)\,f_2(s_2)ds_2 = -\frac{2\pi(1-\nu^2)}{E}\sigma_{yy}^{T}(r_1,t), \qquad -1\le r_1\le 1, \quad (10a)$$

$$\int_{-1}^{1}\left[\frac{1}{s_2-r_2}+\frac{a_2}{2}k_{22}(r_2,s_2)\right]f_2(s_2)ds_2+\int_{-1}^{1}\frac{a_1}{2}k_{21}(r_1,s_1)\,f_1(s_1)ds_1 = -\frac{2\pi(1-\nu^2)}{E}\sigma_{yy}^{T}(r_2,t), \qquad -1\le r_2\le 1, \quad (10b)$$

where the basic unknown variables $f_1(x_1)$ and $f_2(x_2)$ are defined by

$$f_1(x_1)=\frac{\partial v^{(1)}(x_1,0^+)}{\partial x_1}, \quad f_2(x_2)=\frac{\partial v^{(2)}(x_2,0^+)}{\partial x_2}, \quad (11)$$

with $v^{(1)}(x_1, y_1)$ and $v^{(2)}(x_2, y_2)$ being the displacements in the y-direction, x_1, y_1, x_2 and y_2 are coordinates defined by

$$x_1 = x, \quad y_1 = y, \qquad x_2 = x, \quad y_2 = y - h. \quad (12)$$

r_1, s_1, r_2, and s_2 are the normalized coordinates

$$x_1=\frac{a_1}{2}(1+r_1), \quad x_1'=\frac{a_1}{2}(1+s_1), \qquad x_2=\frac{a_2}{2}(1+r_2), \quad x_2'=\frac{a_2}{2}(1+s_2). \quad (13)$$

k_{11}, k_{12}, k_{21} and k_{22} are known kernels given by Feng and Jin[10], and σ_{yy}^{T} is given in Eq. (9).

According to the singular integral equation theory [13], the solutions of Eq. (7) have the following form

$$f_1(r_1)=\frac{F_1(r_1)}{\sqrt{1-r_1}},\qquad f_2(r_2)=\frac{F_2(r_2)}{\sqrt{1-r_2}}, \tag{14}$$

where $F_1(r_1)$ and $F_2(r_2)$ are continuous and bounded functions. Once the solutions of the above integral equations are obtained, the TSIFs at the periodic crack tips can be computed from

$$\begin{aligned} K_I^{(1)*}&=\frac{(1-\nu)K_I^{(1)}}{E\alpha_0\Delta T\sqrt{\pi\, b}}=-\frac{1}{2}\sqrt{\frac{a_1}{b}}F_1(1),\\ K_I^{(2)*}&=\frac{(1-\nu)K_I^{(2)}}{E\alpha_0\Delta T\sqrt{\pi\, b}}=-\frac{1}{2}\sqrt{\frac{a_2}{b}}F_2(1), \end{aligned} \tag{15}$$

where $K_I^{(1)}$ and $K_I^{(2)}$ denote the TSIFs at the tips of the long and short cracks, respectively, $K_I^{(1)*}$ and $K_I^{(2)*}$ are the corresponding nondimensional TSIFs, $\Delta T = T_a$, and α_0 is the coefficient of thermal expansion at $x = 0$. In Eq. (15), $F_1(1)$ and $F_2(1)$ have been normalized by $(1+\nu)\alpha_0\Delta T$.

4. Numerical Results and Discussion

In the numerical examples, we use a graded system of alumina/silicon nitride (Al_2O_3/Si_3N_4) FGM for cutting tools applications to examine the effects of cooling rate on the TSIFs. The FGM is assumed to be a two-phase composite material with graded volume fractions of its constituent phases. The volume fraction of Si_3N_4 is assumed to follow a simple power function

$$V(x)=(x/b)^p, \tag{16}$$

where p is the exponent determining the volume fraction profile. The material properties of the FGM are calculated using conventional micromechanics models [14] and the properties of Al_2O_3 and Si_3N_4 are given in Table 1 [15]. In the numerical calculations, we only consider the loading case of $T_b = 0$ (the initial temperature), which means that only the cracked surface $x = 0$ of the FGM plate is subjected to a temperature drop.

Fig. 2a shows the normalized TSIF $K_I^{(1)*}$ at the tips of the long cracks versus nondimensional time τ for various values of the cooling rate parameter τ_a. The crack spacing is $h/b = 1$, the length of the long cracks is $a_1/b = 0.1$, the crack length ratio is $a_2/a_1 = 0.2$, and the material gradation profile index is $p = 0.5$. The TSIF under the sudden cooling condition ($\tau_a = 0$, and hence infinite cooling rate) is also included. For a given cooling rate (T_a/τ_a), the TSIF initially increases with time, rapidly reaches the peak value and then decreases with time. The peak TSIF decreases dramatically with a decrease in the cooling rate (increasing τ_a). Moreover, the time at which the TSIF reaches its peak increases with a decrease in the cooling rate.

Fig. 2b shows the normalized TSIF $K_I^{(2)*}$ at the tips of the short cracks versus nondimensional time τ. All the geometrical and material gradation parameters are the same as those in Fig. 2a. The TSIF versus time response exhibits similar trend to that at the tips of the long cracks shown in Fig. 2a. Comparing the results in Figs. 2a and 2b, we can see that the peak TSIF at the short crack tip under the sudden cooling condition is about the same as the corresponding value for the long cracks. The peak TSIFs under finite cooling rates (nonzero τ_a), however, are significantly lower than the

corresponding values at the tips of the long cracks.

Table 1. Material properties of Al_2O_3 and Si_3N_4

	Young's modulus (GPa)	Poisson's ratio	CTE (10^{-6}/K)	Thermal conduc-tivity (W/m-K)	Mass density (g/cm^3)	Specific heat (J/g-K)	Fracture toughness (MPa-m$^{1/2}$)
Al_2O_3	320	0.25	8.0	20	3.8	0.9	4
Si_3N_4	320	0.25	3.0	35	3.2	0.7	5

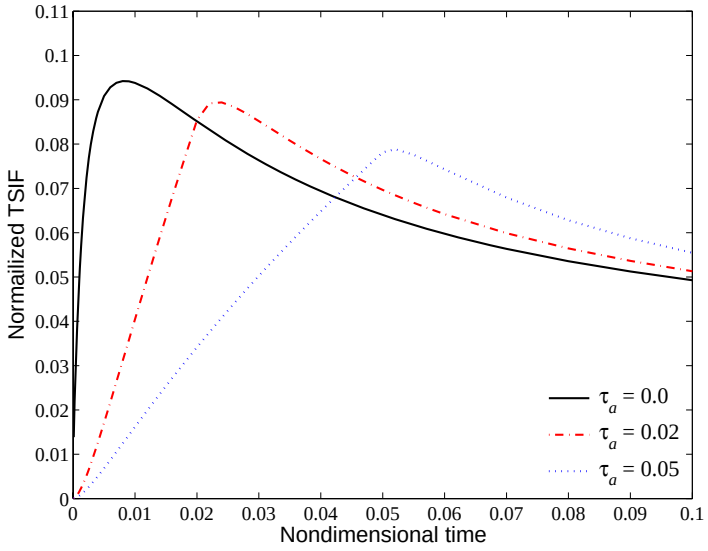

Figure 2a: Normalized TSIF versus nondimensional time at the tips of the long cracks (a_1/b = 0.1, a_2/a_1 = 0.2, h/b = 1.0, p = 0.5)

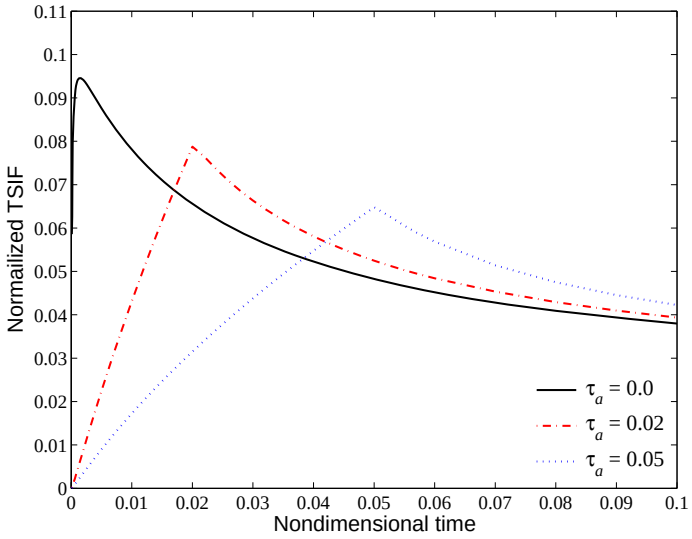

Figure 2b: Normalized TSIF versus nondimensional time at the tips of the short cracks (a_1/b = 0.1, a_2/a_1 = 0.2, h/b = 1.0, p = 0.5)

Figs. 3a and 3b show the normalized TSIFs at the tips of the long and short cracks, respectively, versus nondimensional time τ for a different crack length ratio a_2/a_1 of 0.6. All other parameters are the same as those in Fig. 2. It is seen that the trend of the TSIF versus time is similar to the case of a_2/a_1 = 0.2 shown in Figs. 2a and 2b. The peak TSIFs for the long cracks now are lower than those for a_2/a_1 = 0.2. However, the peak TSIFs for the short cracks are higher than those for a_2/a_1 = 0.2. The decreased peak TISF for the long cracks and the increased peak TSIFs for the short cracks are the results of enhanced interaction between the long and short cracks as the difference in the crack lengths is now smaller.

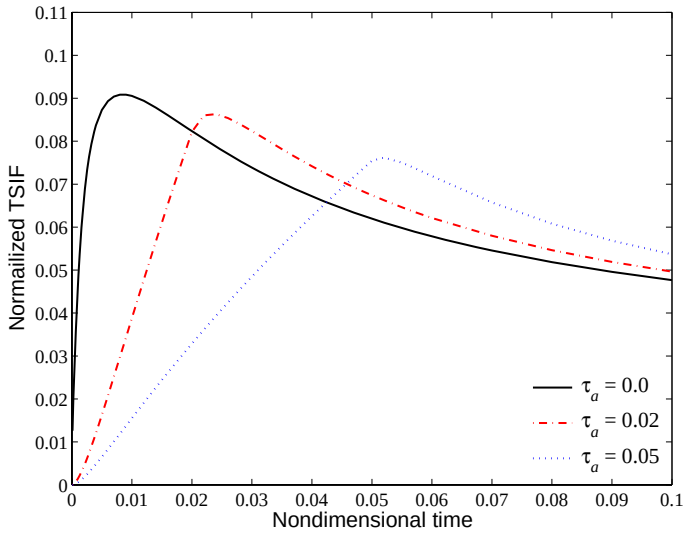

Figure 3a: Normalized TSIF versus nondimensional time at the tips of the long cracks (a_1/b = 0.1, a_2/a_1 = 0.6, h/b = 1.0, p = 0.5)

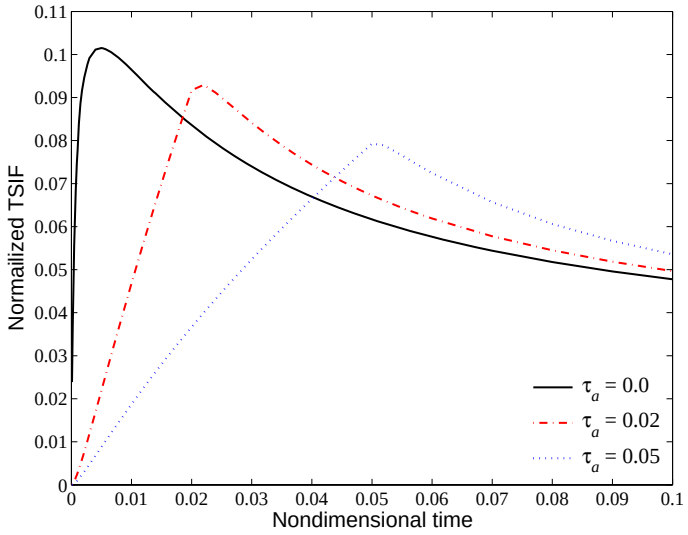

Figure 3b: Normalized TSIF versus nondimensional time at the tips of the short cracks (a_1/b = 0.1, a_2/a_1 = 0.6, h/b = 1.0, p = 0.5)

5. Concluding Remarks

This work is focused on the effects of cooling rate on the thermal stress intensity factors (TSIFs) at the tips of parallel edge cracks of alternating lengths in an FGM plate. The cooling rates at the surfaces of the FGM plate are described by a linear ramp function. The TSIFs are obtained using a closed-form, short-time temperature solution and an integral equation method. Numerical results for an Al_2O_3/Si_3N_4 FGM system show that the peak TSIFs at the tips of both long and short cracks decrease with a decrease in cooling rate. The variations of the peak TISF for the long and short cracks with the cooling rate and crack length ratio exhibit a complex pattern due to the interactions between the long and short cracks.

References

[1] A. Kawasaki, R. Watanabe, Fabrication of disk-shaped functionally gradient materials by hot pressing and their thermomechanical performance, in: J.B. Holt, M. Koizumi, T. Hirai, Z.A. Munir (Eds.), Ceramic Transactions, Vol. 34, American Ceramic Society, Westerville, OH, 1993, pp. 157–164.

[2] K. Kokini, J. DeJonge, S. Rangaraj, B. Beardsley, Thermal shock of functionally graded thermal barrier coatings, in: K. Trumble, K. Bowman, I. Reimanis,S. Sampath (Eds.), Ceramic Transactions, Vol. 114, American Ceramic Society, Westerville, OH, 2001, pp. 213-221.

[3] S. Rangaraj, K. Kokini, Multiple surface cracking and its effect on interface cracks in functionally graded thermal barrier coatings under thermal shock. ASME Journal of Applied Mechanics, 70 (2003) 234-245.

[4] H.C. Han, B.L. Wang, Thermal shock resistance enhancement of functionally graded materials by multiple cracking. Acta Materialia, 54 (2006) 963-973.

[5] Z.H. Jin, Y.Z. Feng, Thermal fracture resistance of a functionally graded coating with periodic edge cracks. Surface & Coatings technology, 202 (2008) 4189-4197.

[6] Z.H. Jin, Y.Z. Feng, Effects of multiple cracking on the residual strength behavior of thermally shocked functionally graded ceramics. International Journal of Solids and Structures, 45 (2008) 5973-5986.

[7] S. Nemat-Nasser, L.M. Keer, K.S. Parihar, Unstable growth of thermally induced interacting cracks in brittle solids. International Journal of Solids Structures, 14 (1978) 409-430.

[8] H.A. Bahr, H.J. Weiss, H.G. Maschke, F. Meissner, Multiple crack propagation in a strip caused by thermal shock. Theoretical and Applied Fracture Mechanics, 10 (1988) 219-226.

[9] Z.H. Jin, Y.Z. Feng, An array of parallel edge cracks with alternating lengths in a strip subjected to a thermal shock. Journal of Thermal Stresses, 32 (2009) 431-447.

[10] Y.Z. Feng, Z.H. Jin, Thermal fracture of a functionally graded plate with parallel surface cracks. Acta Mechanica Solida Sinica, 22 (2009) 453-464.

[11] Y.Z. Feng, Z.H. Jin, Thermal shock damage and residual strength behavior of a functionally graded plate with surface cracks of alternating lengths. Journal of Thermal Stresses, 35 (2012) 30-47.

[12] Z.H. Jin, Heat conduction in a functionally graded plate subjected to finite cooling/heating rates: An asymptotic solution. Materials, 4 (2011) 2108-2118.

[13] F. Erdogan, G.D. Gupta, T.S. Cook, Numerical solution of singular integral equations, in: G.C. Sih (ed.), Mechanics of Fracture, Vol. 1: Methods of Analysis and Solutions of Crack Problems, Noordhoff International Publishing, Leyden, The Netherlands, 1973.
[14] R.M. Christensen, Mechanics of Composite Materials, John Wiley & Sons, New York, 1979.
[15] D. Munz, T. Fett, Ceramics, Springer, Berlin, 1999.